

Thermals with background rotation and stratification

By KARL R. HELFRICH

Department of Physical Oceanography, Woods Hole Oceanographic Institution,
Woods Hole, MA 02543, USA

(Received 29 January 1993 and in revised form 16 July 1993)

Scaling analysis and experiments are used to study the evolution of thermals in the presence of background rotation. When the ambient environment is homogeneous, the thermal rises and expands until it reaches a critical height where the Rossby number becomes ~ 1 . The thermal then stops expanding and rises in a column. Both the critical height and column radius scale with $(F_0 f^{-2})^{\frac{1}{2}}$. F_0 is the initial thermal buoyancy and f is the Coriolis frequency. The thermal vertical velocity is independent of f . When the background is stratified with buoyancy frequency N , the thermal rises to a neutral buoyancy level which scales with $(F_0 N^{-2})^{\frac{1}{2}}$. For $N/f < 0.6$ column formation occurs before the thermal reaches the neutral level. For $N/f > 0.6$ the thermal reaches the neutral level before rotation is important. In both regimes, geostrophic adjustment eventually causes the formation of a baroclinic vortex consisting of an anticyclonic lens of thermal fluid at the neutral level and cyclonic circulation below. The lens has $Nh/fl \sim 1$. The lens thickness $2h$ and the radius l obey relations of the form $(F_0 N^{-2})^{\frac{1}{2}}(N/f)^m$. However, the exponents m are different in the two regimes. The relevance of these results to deep-ocean convection and hydrothermal venting is discussed.

1. Introduction

There are several important ocean processes in which penetrative convection occurs on spatial and temporal scales such that rotational effects should be significant. In deep convection, strong surface cooling over a broad region produces dense water which can descend to great depths. Observations in the Mediterranean (Stommel, Voorhis & Webb 1971; Schott & Leaman 1991) show that dense water sinks in narrow (~ 1 km diameter) chimneys with downward velocities of ~ 10 cm s $^{-1}$. There is evidence that the convection region, composed of numerous chimneys, will break up into geostrophic eddies with diameters ~ 5 km (Gascard 1978).

Recent scaling analyses and laboratory studies by Fernando, Chen & Boyer (1991) and Maxworthy & Narimousa (1993), and numerical work by Jones & Marshall (1993) have illustrated this interplay of convection and rotation for the case of distributed buoyancy source into an initially homogeneous fluid. They found that surface cooling produces a dense turbulent layer that descends (ascends, in the Fernando *et al.* experiments since they used heating from below), unaffected by rotation until a time, $t \sim f^{-1}$, when the Rossby number of the turbulent flow $u/fl \sim 1$. Here u and l are velocity and length scales of the dominant turbulent motions, and f is the Coriolis parameter. The turbulent layer reaches a depth

$$z_c \sim (B_0 f^{-3})^{\frac{1}{2}},$$

after which, further penetration is controlled by rotation. B_0 is the surface buoyancy flux per unit area. Under rotational control, the fluid descends in columns with diameter

$$l_c \sim (B_0 f^{-3})^{\frac{1}{2}}.$$

Once the columns reach the bottom, the combined effects of radial inflow near the surface and outflow of dense water at the bottom produce a geostrophic flow that is baroclinically unstable. The instability leads to the breakup of the rim of the convecting region into geostrophic eddies with radius D that scales as (Maxworthy & Narimousa 1993)

$$D/H \sim [B_0/f^3 H^2]^{\frac{1}{4}}.$$

H is the total depth. These scaling arguments are supported by laboratory and numerical work and illustrate the important interaction of convection and background rotation.

Hydrothermal venting is another oceanic process in which convection and rotation interact. Venting often occurs as isolated high-temperature vents known as black smokers from which hot water (temperatures in excess of 300 °C) rises as a turbulent plume until entrainment and ambient stratification cause the plume to spread laterally at a level of neutral buoyancy. Although the rising phase is quite rapid, and scales with N^{-1} , the spreading phase is affected by rotation on the typically slower timescale f^{-1} . Here N is the background buoyancy frequency. Rotation inhibits the lateral spreading of plume fluid and leads to anticyclonic flow at the neutral level and cyclonic flow, driven by entrainment into the rising plume, below. A theoretical model (Speer 1989) and laboratory experiments (Helfrich & Battisti 1991) support this picture of plume-driven baroclinic vortex formation. The experiments also demonstrate that once the plume radius grows to exceed about one Rossby radius ($\sim NZ_M/f$, where Z_M is the height of the neutral level), the plume vortex becomes unstable. This results in unsteady generation of baroclinic vortices from a steady source.

Large eddy-like lenses of water with hydrothermal chemical and thermal signatures, termed megaplumes, are suggested to result from the rapid release of large volumes of hydrothermal fluid resulting from seafloor volcanic activity (Baker *et al.* 1989; Chadwick, Embley & Fox 1991). The final megaplume state might depend on the interaction of a 'thermal' (i.e. the sudden release of a mass of buoyant fluid) with a rotating stratified ocean.

Some previous experimental work on thermals in homogeneous rotating systems has been reported. Elrick (1979) found that the rotation increases the rate of ascent of the thermal and inhibits the volumetric growth when compared to the non-rotating case. However, Wilkins *et al.*'s (1969) experiments showed that the rate of ascent was not affected by rotation. Both studies considered just a few experiments and did not find any general scaling laws of the type found for the deep-convection work. Wilkins *et al.* did derive a modified version of the standard thermal theory, but the comparison with the few experiments is not convincing. The theory required the introduction of several new and unknown parameters.

In this paper the evolution of thermals in homogeneous rotating systems is re-examined and extended to include the effects of background stratification. Isolated thermals were chosen since they are the simplest convective elements from which intuition can be built about more complicated situations (such as large distributed sources, which introduce an additional lengthscale). Furthermore, thermals are analogues of rapid-release hydrothermal events. Since observations of the water column structure (i.e. long-lived megaplumes) are easier to obtain than observations of the actual tectonic or volcanic event, it is worthwhile to understand how megaplumes

might be related to their source characteristics such as total buoyancy release, source geometry, etc.

In §2 thermal evolution in non-rotating homogeneous and stratified systems is reviewed. A dynamical scaling theory is developed for thermals in homogeneous rotating systems and then extended to the stratified situation. Laboratory experiments that support the proposed scalings and permit the determination of unknown coefficients are discussed in §3. For the unstratified case thermal growth is arrested when the Rossby number is ~ 1 . The thermal then falls as a constant-radius Taylor column. When the environment is weakly stratified, column formation occurs before the thermal reaches the neutral buoyancy level. For strong stratification the thermal reaches the neutral level prior to feeling the effects of rotation. In either stratified case, subsequent geostrophic adjustment leads to formation of a baroclinic vortex pair consisting of an anticyclonic lens at the neutral level and cyclonic flow above. However, the lens thickness, radius, and stability criterion obey different scaling relations in these two regimes. These results are summarized and discussed in §4.

2. Thermal scaling

2.1. Thermals without rotation

The basic dimensional analysis and theory for thermals in homogeneous or stratified environments were developed by Morton, Taylor & Turner (1956), and are summarized in Turner (1973, 1986). Only a brief review is given here. An initially still thermal rises into a homogeneous fluid as a roughly spherical mass which expands by turbulent entrainment as it rises. Conservation equations for mass, momentum, and buoyancy can be written assuming self-similar evolution of the thermal. However, the features of most significance here can be deduced from dimensional analysis. This leads to the following dependencies of rise height z , thermal radius b , vertical velocity $w = dz/dt$, and reduced gravity of the thermal g' on time t :

$$z = k_1 F_0^{1/3} t^{1/2}, \quad (1)$$

$$b = k_2 F_0^{1/3} t^{1/2}, \quad (2)$$

$$w = k_3 F_0^{1/3} t^{-1/2}, \quad (3)$$

$$g' = k_4 F_0^{1/3} t^{-3/2}, \quad (4)$$

where k_n ($n = 1-4$) are constants and

$$F_0 = V_0 g' \quad (5)$$

is the initial thermal buoyancy. Here V_0 is the initial thermal volume, $g'_0 = g(\rho_a - \rho_0)/\rho_a$ is the initial reduced gravity, g is the acceleration due to gravity, ρ_a is the density of the ambient environment and ρ_0 is the initial density of the thermal. The buoyancy $\frac{4}{3}\pi b^3 g'$ of the evolving thermal is constant and equal to F_0 .

From (1) and (2) it is clear that the radius and height are linearly related,

$$b = \alpha z. \quad (6)$$

The constant α is the entrainment coefficient. Scorer's (1957) laboratory experiments with salt-water thermals released into fresh water gave $\alpha = 0.25$, though the value varied between experiments. The entrainment coefficient is dependent upon details of the thermal release mechanism and whether the thermal is in a self-similar turbulent state from the beginning (Turner 1973; Sanchez *et al.* 1989). Scorer also determined the constants k_n in (1)–(4) to be

$$(k_1, k_2, k_3, k_4) \approx (2.4, 0.6, 1.2, 1.6). \quad (7)$$

A thermal in a homogeneous environment rises indefinitely. In a stably stratified environment, the thermal buoyancy is continuously reduced until the thermal stops rising and spreads laterally at a level of neutral buoyancy, Z_M . Again, models based on self-similarity and dimensional arguments have been used to deduce (Morton *et al.* 1956; Turner 1973)

$$Z_M \propto \alpha^{-\frac{3}{4}} F_0^{\frac{1}{4}} N^{-\frac{1}{2}}. \quad (8)$$

Here F_0 is defined using the ambient density at the initial level of the thermal and N is the constant buoyancy frequency of the ambient environment. Experiments by Morton *et al.* (1956) gave $\alpha \approx 0.25$, and

$$Z_M = 2.66 F_0^{\frac{1}{4}} N^{-\frac{1}{2}} = 2.66 l_N. \quad (9)$$

The stratification lengthscale $l_N = (F_0 N^{-2})^{\frac{1}{4}}$. The thermal radius grows linearly with height over a distance of about $\frac{2}{3} Z_M$. The thermal then begins to flatten out as Z_M is approached and ultimately spreads out as an axisymmetric intrusion.

2.2. Thermals with rotation

The introduction of background rotation with Coriolis frequency f introduces a new timescale $t_f \sim f^{-1}$ into the problem. For times greater than t_f , the effect of rotation begins to influence thermal evolution. More precisely, once the Rossby number

$$\epsilon \equiv u/fl \sim 1, \quad (10)$$

rotation will affect the thermal evolution. Here u is a velocity scale and l a lengthscale of the dominant turbulent motions within the thermal. Taking u to scale with w , the thermal fall velocity (3), and $l \approx b$, the thermal radius (2), then (10) gives an estimate for t_f ,

$$t_f \approx 2f^{-1}. \quad (11)$$

Here (7) has been used to estimate the constant.

For thermals in a homogeneous system, aspects of evolution beyond this time can be anticipated from results of Maxworthy & Narimousa (1993), Fernando *et al.* (1991) and Jones & Marshall (1993). Once rotation becomes significant, the lateral spread of the thermal is arrested and geostrophic circulation established. This occurs at a height z_R , after which the thermal rises in a column with radius b_R . Estimates for z_R and b_R are, from (1) and (2) evaluated with t_f from (11),

$$z_R \approx 3.6(F_0 f^{-2})^{\frac{1}{4}} = 3.6 l_f, \quad (12)$$

$$b_R \approx 0.9 l_f. \quad (13)$$

Here $l_f = (F_0 f^{-2})^{\frac{1}{4}}$ is the rotational lengthscale. The constants are estimated using (7). Similar scales for reduced gravity $g'_R \sim (F_0 f^6)^{\frac{1}{4}}$ and velocity $w_R \sim (F_0 f^2)^{\frac{1}{4}}$ can be found. Thermal-driven entrainment prior to t_f generates a cyclonic circulation in the region $z < z_R$ as ambient fluid moves radially inward to replace fluid entrained and carried away by the thermal. Once the Taylor column has been established, lateral entrainment is probably reduced and the thermal may rise more rapidly than the non-rotating case as Elrick's (1979) experiments suggest.

When the ambient fluid is stratified, the problem is complicated by the presence of both the rotational timescale $t_f \sim f^{-1}$ and the buoyancy timescale $t_N \sim N^{-1}$. This latter timescale is the time for the thermal to reach the equilibrium level Z_M in the case of no rotation. Thermal behaviour can be considered in two limits of the ratio $t_f/t_N \approx N/f$.

For $N/f \gg 1$ the rising thermal reaches the neutral buoyancy level well before rotational effects become important. The thermal then begins to spread laterally as an

axisymmetric intrusion until $t \sim f^{-1}$ when geostrophic adjustment limits the lateral spreading, resulting in an anticyclonic lens of thermal fluid with radius l and thickness $2h$. Gill's (1981) theory for homogeneous intrusions suggests that the final thermal lens has a Burger number

$$Nh/fl \sim 1. \tag{14}$$

Entrainment into the rising thermal again results in cyclonic circulation in the region below the anticyclonic lens. The result is a baroclinic vortex pair extending over a depth $\sim Z_M$.

Radius l and thickness $2h$ of the lens, as well as a vortex stability criterion, can be derived based on conservation of mass and (14). As the thermal reaches the neutral buoyancy level, it has a radius $\sim \alpha Z_M$ and a volume $\sim \frac{4}{3}\pi(\alpha Z_M)^3$. Equating this volume with the volume of an axisymmetric ellipsoidal eddy of thickness $2h$ and radius l gives

$$(\alpha Z_M)^3 \sim hl^2. \tag{15}$$

Use of (14) gives $l = k_5 l_N (N/f)^{\frac{1}{3}}, \tag{16}$

$$h = k_6 l_N (N/f)^{-\frac{2}{3}}. \tag{17}$$

If the Burger number (14) is taken equal to one, $\alpha = 0.25$ and Z_M to be given by (9), then the constants $k_5 = k_6 \approx 2.66\alpha \approx 0.7$.

Quasi-geostrophic stability theory for two-layer axisymmetric vortices suggests that the baroclinic vortex is unstable for $l/L_R \gtrsim 1$ and will break into two or more smaller vortex pairs (Helfrich & Send 1988). Here L_R is the internal Rossby deformation radius, which for a vortex pair of total height Z_M is

$$L_R = NZ_M/f. \tag{18}$$

From (16) and (18) $l/L_R = lf/NZ_M \approx \alpha(N/f)^{-\frac{2}{3}}, \tag{19}$

using the estimate for k_5 given above. Thus for $N/f \gg 1$, the vortex pair is expected to be stable.

In the weak stratification limit, then $N/f \ll 1$, the thermal is affected by rotation prior to the effects of stratification (i.e. before the neutral buoyancy level is reached). Since the early stages ($t \ll t_N$) of thermal evolution in stratified systems are essentially identical to the non-stratified case, it is expected that the thermal forms a columnar structure with a radius that scales with l_f . The fluid rises within the column until further penetration is arrested by stratification. The depth to which the thermal ascends is not necessarily Z_M , but since stratification must eventually limit penetration, this depth should scale with l_N .

Following the analysis for $N/f \gg 1$, it is expected that geostrophic adjustment leads to a baroclinic vortex pair with an anticyclonic lens of thermal fluid at a level $z \sim l_N$, and a cyclonic vortex below. The volume of thermal fluid which forms the vortex scales with $l_f^2 l_N$. Assuming that the anticyclonic lens has a thickness $2h$ and radius l with $Nh/fl \sim 1$, then volume conservation gives

$$l \sim l_N (N/f)^{\frac{2}{3}}, \tag{20}$$

$$h \sim l_N (N/f)^{-\frac{1}{3}}. \tag{21}$$

This is similar to the strong stratification limit ((16) and (17)) with the exception of the powers of N/f . The stability of the adjusted vortex should again depend on

$$l/L_R \sim lf/Nl_N \sim (N/f)^{-\frac{1}{3}}. \tag{22}$$

Thus for $N/f \ll 1$ it is likely that $l/L_R > 1$ for some critical N/f and the vortex is unstable. Of course, this analysis depends on the constants that are implied in (20), (21), and (22).

Scaling in the regime $N/f = O(1)$, as well as the ranges of validity of the above two limits, is not clear *a priori*. Thus laboratory experiments were undertaken to test these scaling arguments and to determine their ranges of validity and the coefficients necessary for their general application.

3. Experiments

3.1. Experimental method

The experiments were conducted in a glass tank measuring $61 \times 61 \times 60$ cm deep mounted on a rotating turntable. The tank was filled with either fresh water or a salt-stratified system of constant N using the two-tank filling method. In all of the experiments the fluid depth was 45 cm. In the stratified runs N was determined by withdrawing six samples of water at known depths from 0 to 30 cm and measuring their density with an electronic densimeter. The resulting profiles were consistently linear.

The thermal fluid was a salt solution, dyed for flow visualization. The thermals were heavy and fell. The fluid was introduced by quickly inverting a horizontally positioned half-cylinder of diameter 1.5 cm and either 1.5 or 2.0 cm length. The cylinder was positioned so that the level of fluid in the cylinder was equal to the tank level. This traditional method of thermal initiation does introduce some initial circulation within the thermal, but results in the rapid approach to a self-similar turbulent state. Other methods that result in an initially motionless thermal lead to initial behaviour that is significantly different from the non-rotating similarity theory (Sanchez *et al.* 1989). Thermal evolution was recorded using still (35 mm) and video cameras. The images were corrected for optical distortion to obtain quantitative information on thermal kinematics.

The initial volume V_0 was either 2.5 ml (with the 1.5 cm long cylinder) or 5 ml (with the 2 cm long cylinder). In the experiments reported below, there was no discernible dependence on the size of the cylinder. The initial density difference was in the range $(\rho_0 - \rho_a)/\rho_0 = 0.04-0.20$. The Coriolis parameter $f = 0.83-2.5 \text{ s}^{-1}$ for the unstratified experiments. Thus $F_0 f^{-2}$ was investigated in the range $20-650 \text{ cm}^4$ giving $l_f = (F_0 f^{-2})^{1/4} = 2.1-5.1 \text{ cm}$.

For the stratified experiments, V_0 and F_0 were the same as above. The Coriolis frequency f was varied in the range $0.1-1.65 \text{ s}^{-1}$ and N $0.3-0.9 \text{ s}^{-1}$. Values of $N/f = 0.16-4.86$ were investigated. The experiments were arranged so that the expected maximum penetration $Z_M = 13-20 \text{ cm}$. Experiment size considerations limited the range. For example, for large N/f the resulting vortex would, according to (16), increase in radius directly proportionally to $l_N (\propto Z_M)$ and thus could become large enough that the tank size becomes important. Care was taken to avoid this situation.

The Reynolds number for the thermals can be estimated using b and w from the standard thermal scaling ((2) and (3)). This gives

$$R = wb/\nu = k_2 k_3 F_0^{1/2} / \nu.$$

For these experiments $R = 300-500$. These values are small, but early thermal evolution agreed with the non-rotating inviscid scaling and previous experiments. Because of this agreement, it appears that viscosity does not exert a controlling influence on the turbulent thermal regime. The long-time spin-down of the plume-produced vortices will be affected by viscosity, but the focus here is on the turbulent convection and initial vortex structure.

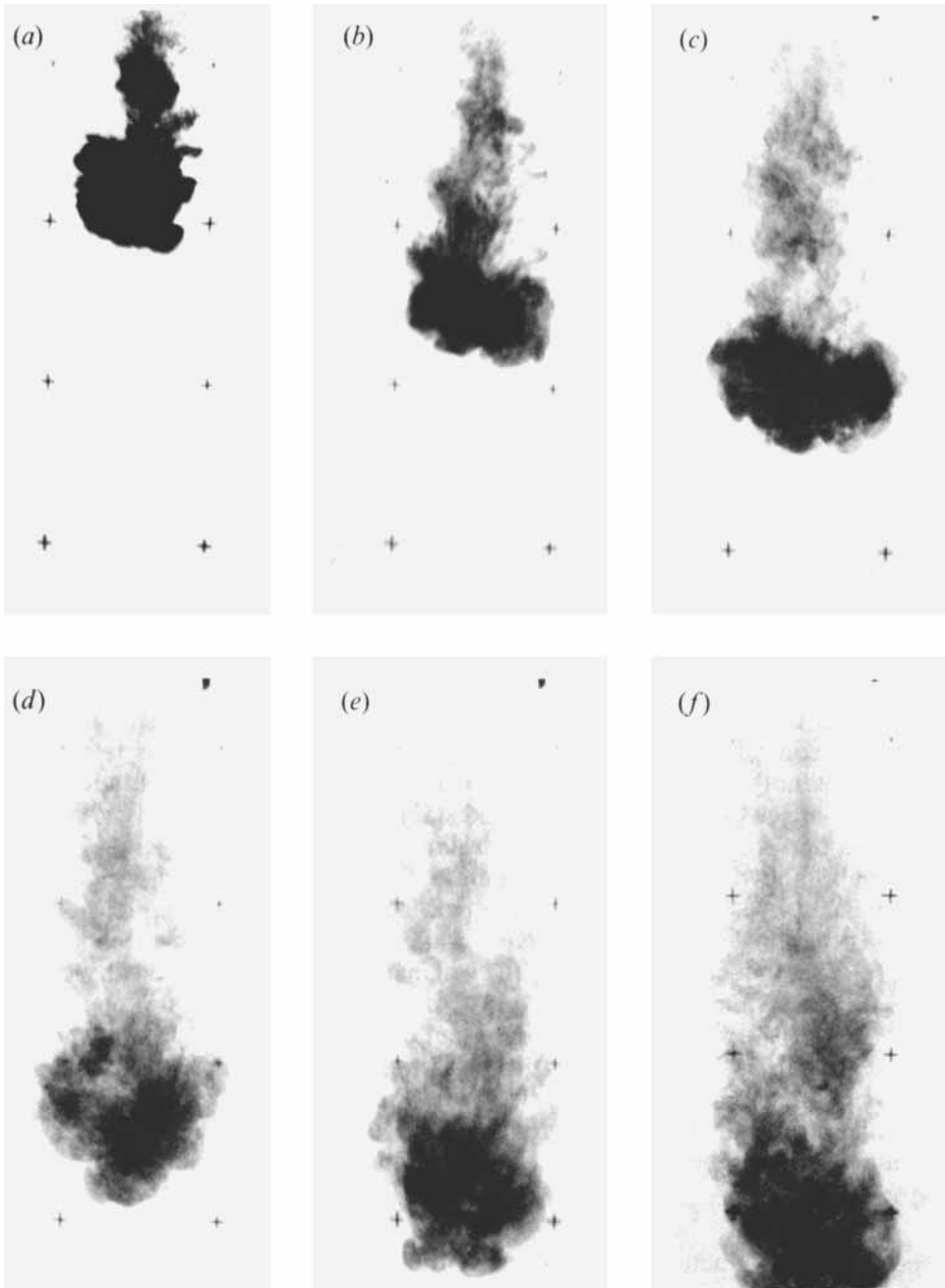


FIGURE 1. Sequence of photographs showing thermal evolution in an unstratified environment for $(F_0 f^{-2})^{\frac{1}{2}} = 3.98$ cm. Time increases from (a) to (f).

3.2. Unstratified experiments

Figure 1 shows a sequence of sideview photographs for an experiment with $l_f = 3.98$ cm. The first three frames show the early evolution before rotation becomes important. The effects of rotation are evident in frames (d), (e), and (f). The thermal radius remains nearly constant and the front falls to form a columnar structure. Fluid appears to detrain from the rear of the thermal and mix within the column. Observations of dye

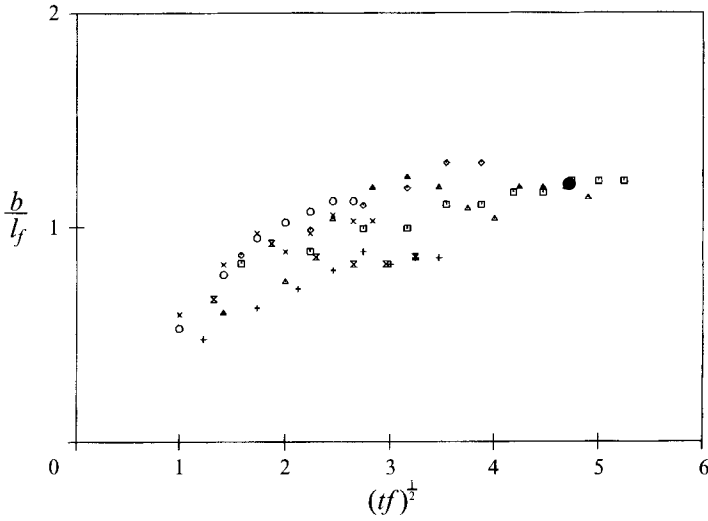


FIGURE 2. Normalized thermal radius b/l_f evolution for several runs spanning the parameter range studied. The symbols are: \square , $(l_f, f) = (2.11 \text{ cm}, 2.50 \text{ s}^{-1})$; \triangle , $(2.36, 2.0)$; $+$, $(3.23, 1.5)$; \times , $(3.96, 1.0)$; \diamond , $(2.95, 2.5)$, \times , $(3.52, 1.75)$; \circ , $(4.67, 1.0)$.

streaks show that the horizontal circulation in the column is weak and anticyclonic below the depth of column formation and stronger and cyclonic above. On a long timescale the column collapses and undergoes geostrophic adjustment to form an anticyclonic conical eddy of thermal fluid on the tank bottom. This later stage of evolution has not been studied here, but it is similar to Griffiths & Linden's (1981) experiments of geostrophic adjustment and stability of vortices formed by the sudden release of a buoyant column fluid under rotation.

The temporal evolution of the maximum thermal radius is shown in figure 2. The figure includes several runs spanning the parameter range. The data are normalized using the rotation lengthscale $l_f = (F_0 f^{-2})^{1/4}$ and f^{-1} . According to the non-rotating scaling (2), the data should fall on a line originating near $b = 0$. The early evolution follows this behaviour; however, once $tf \gtrsim 4$, the radii become nearly constant with $b/l_f \approx 1$. There is some scatter in the data, but examination of all the runs shows that the scatter does not depend systematically on the external parameters. The scatter is indicative of the variability of the process and the experimental error.

A similar plot of the penetration depth z , defined as the distance from the source to the leading edge of the thermal, is shown in figure 3 for the same runs. The data collapse to a line

$$z/l_f \approx 2.7(tf)^{1/2}. \quad (23)$$

The penetration characteristics do not seem to be affected by rotation even though the thermal lateral expansion is halted for $tf \gtrsim 4$. The velocity of the thermal $w = dz/dt$, is

$$w/(F_0 f^2)^{1/4} \approx 1.35(tf)^{-1/2}. \quad (24)$$

Note that f can be eliminated from (24), thus w is independent of f . The constant in (24) is slightly greater than Scorer's value of 1.2 (see (3) and (7)). This increase is probably due to some detail of these particular experiments (see discussion below) and not rotation since (24) is independent of f .

The Rossby number (10) at $tf \approx 4$ when rotation inhibits spreading is

$$\epsilon = w/fb \approx 0.7,$$

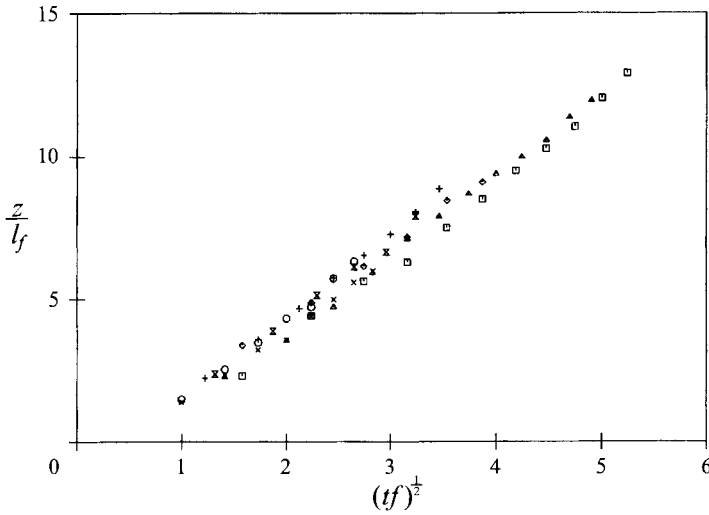


FIGURE 3. Same as figure 2 except penetration depth z is shown.

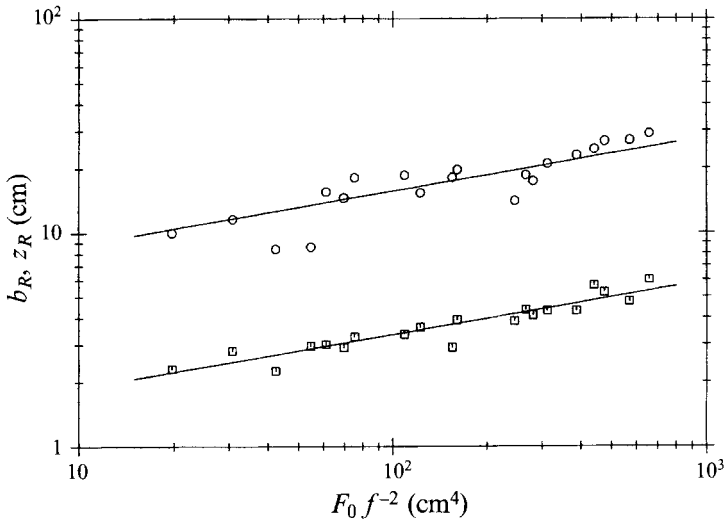


FIGURE 4. The thermal radius b_R (\square) and depth z_R (\circ) at the point of column formation. The solid lines show the best fits of the assumed scalings, (25) and (26).

using (24) and $b \approx l_f$.

In figure 4 the radius b_R and depth z_R of the thermal at the time of column formation are shown plotted against $F_0 f^{-2}$ for all the runs. Also shown are best-fit curves,

$$b_R = 1.05(F_0 f^{-2})^{1/4}, \tag{25}$$

and

$$z_R = 4.94(F_0 f^{-2})^{1/4}, \tag{26}$$

of the proposed scaling ((12) and (13)). The data for the radius b_R show little scatter. The coefficient of 1.05 in (25) is close to the *a priori* estimate of 0.9 in (13). The data for z_R are slightly more scattered, though the overall trend is good. Fitting the data without constraining the exponent to $\frac{1}{4}$ gives a coefficient of 1.03 and an exponent of 0.25 for b_R and 3.67 and 0.31, respectively, for z_R .

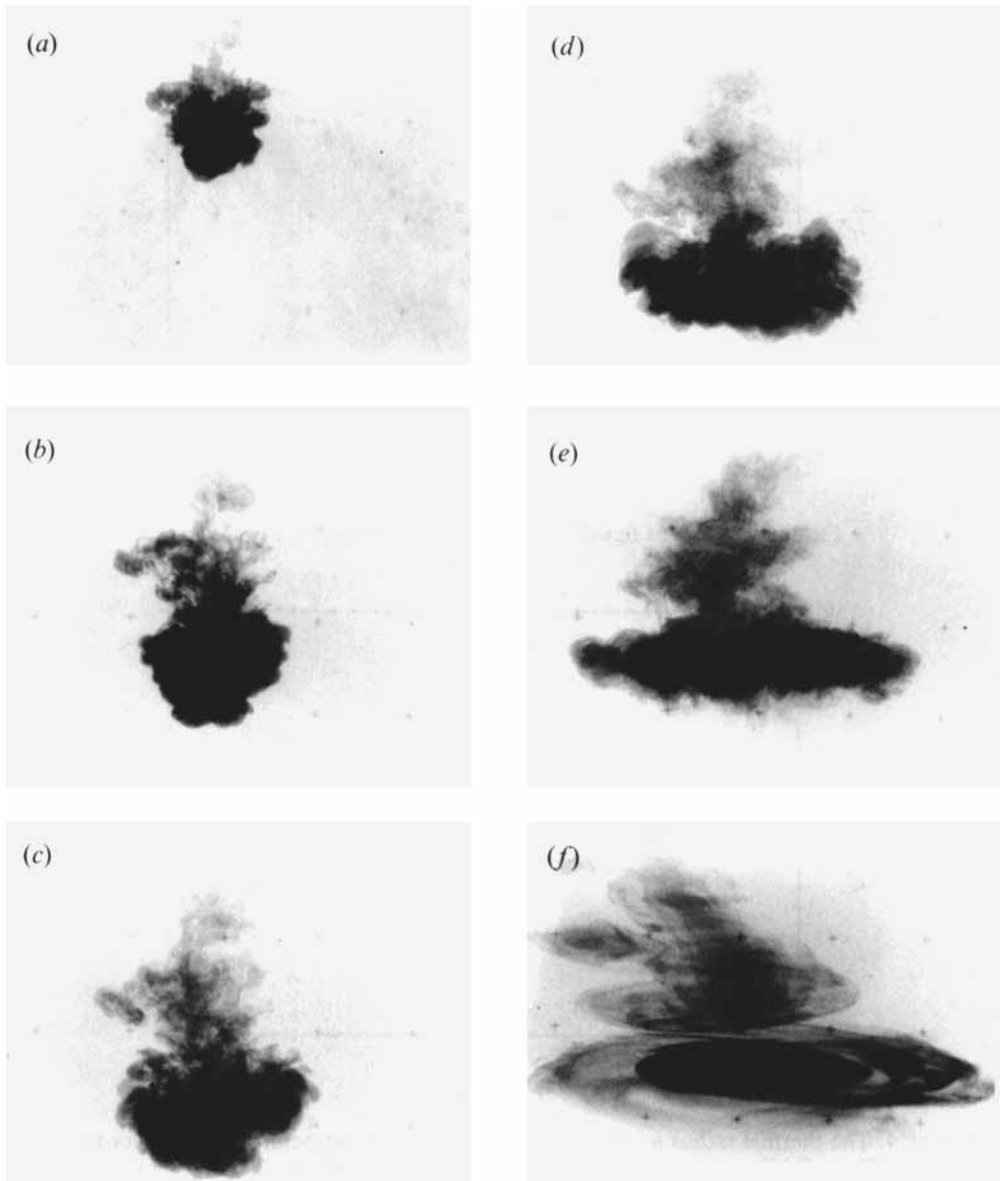


FIGURE 5. Sequence of photos showing thermal evolution for a run with $N/f = 4.62$. Time increases for (a) to (f). The thermal falls to the neutral level before being affected by rotation.

The ratio $b_R/z_R \approx 0.2$ (from (25) and (26)) implies an entrainment coefficient $\alpha \approx 0.2$ for the thermal up to the point of column formation. This is slightly lower than the standard value of $\alpha = 0.25$ (Turner 1973, 1986). This is probably due to details of the thermal release. Thermals with an initial circulation show a smaller effective entrainment coefficient (Turner 1973).

3.3. Stratified experiments

Thermal evolution in a rotating, strongly stratified environment is shown in figure 5 for $N/f \approx 4.62$. The thermal descends and grows (frames a and b) until it reaches the neutral level (frames c and d) and begins to spread laterally. There is some initial

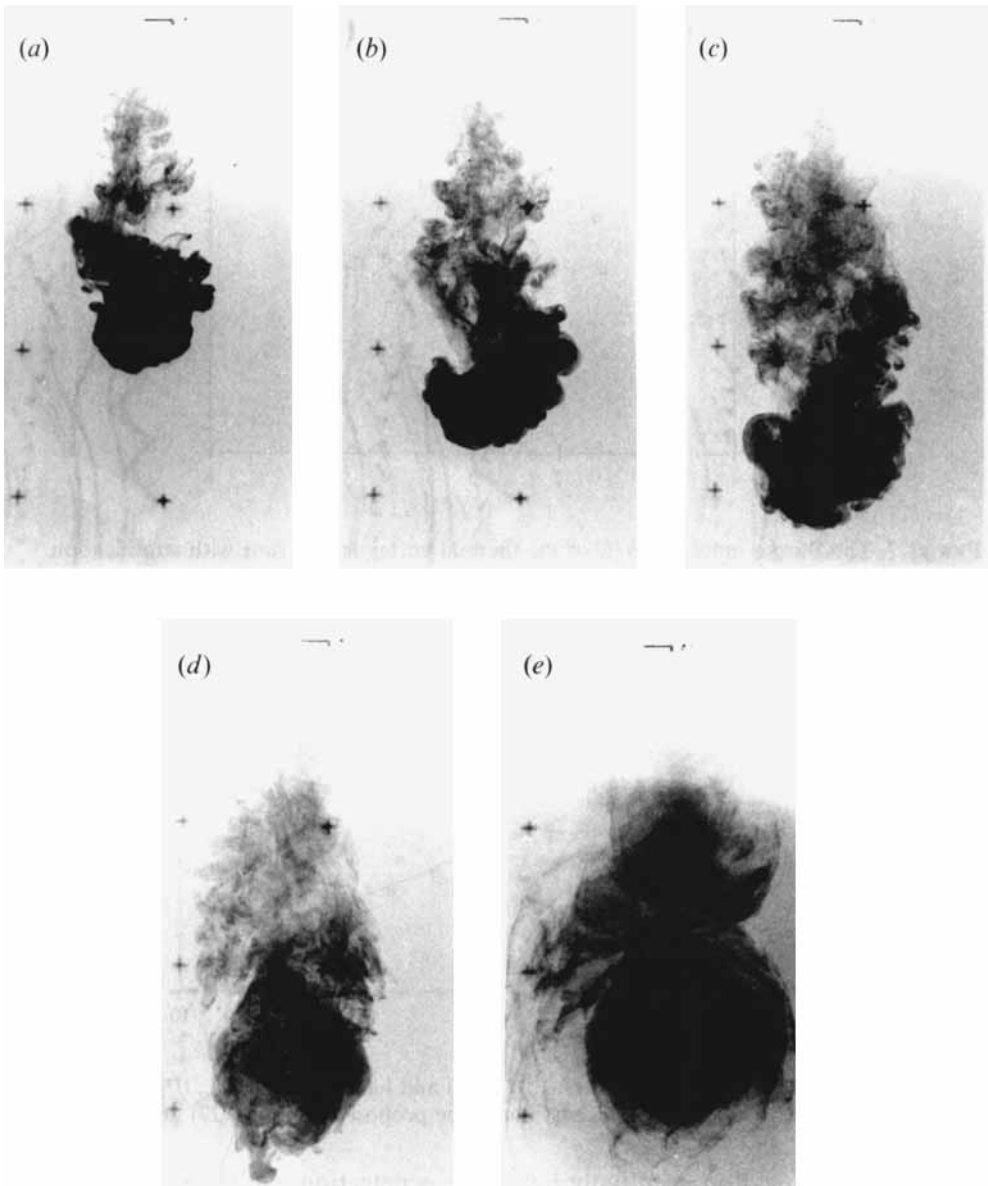


FIGURE 6. Sequence of photos for $N/f = 0.40$. Time increases from (a) to (e). Thermal evolution is affected by rotation before the thermal reaches the neutral level.

overshoot of this level. In frame (e) rotation begins to inhibit the spreading until an anticyclonic lens is formed (frame *f*). Organization of flow above the lens is evident. Dye streaks show that this region is circulating cyclonically. The fluid immediately below the anticyclonic lens has a very weak anticyclonic circulation due to the compression of ambient isopycnals by the lens. The baroclinic vortex remained stable for the duration of the experiment.

When $N/f \ll 1$, the scaling analysis suggests that rotation influences thermal evolution before the thermal reaches the neutral buoyancy level. An example of an experiment for $N/f = 0.40$ is shown in figure 6. In frames (a)–(c), the thermal lateral expansion is halted and, similar to the non-stratified runs, a column is formed.

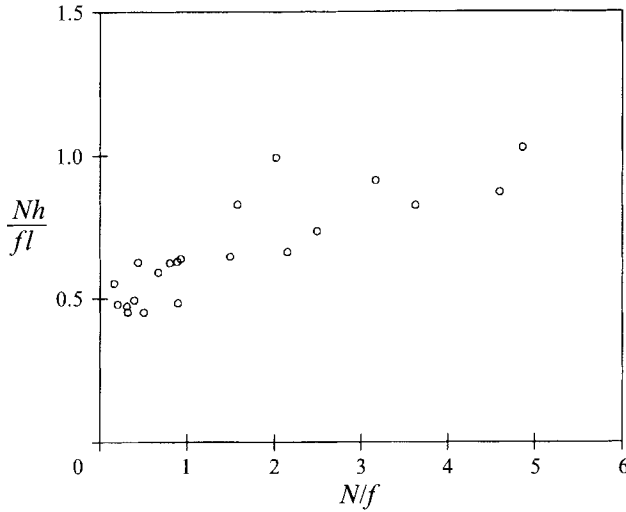


FIGURE 7. The Burger number Nh/fl of the thermal vortex for all runs with stratification.

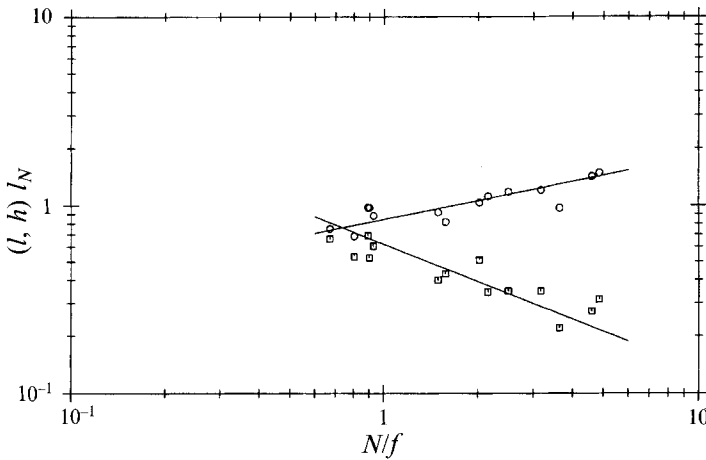


FIGURE 8. Normalized thermal vortex radius l/l_N (\circ) and half-thickness h/l_N (\square) for the runs with $N/f > 0.6$. The lines are the best fits of the proposed scalings, (27) and (28).

However, the stratification eventually limits the penetration. Collapse of the column and subsequent geostrophic and adjustment (frames *d* and *e*) result in an anticyclonic vortex of thermal fluid at the neutral level with cyclonic flow above. This baroclinic vortex is also stable.

One of the assumptions of the scaling analysis is that the Burger number Nh/fl of the thermal lens to be a constant of order one. Figure 7 shows the observed Burger numbers (measured immediately after the geostrophic adjustment was complete and the turbulence had decayed away) for all the experiments. There is a tendency for Nh/fl to increase from about 0.5 to 0.9 as N/f increases. Values in this range are consistent with Helfrich & Battisti (1991) who found $Nh/fl = 0.5-1.0$ for vortices formed by continuous point-source plumes.

When $N/f \gg 1$, the scaling analysis ((16) and (17)) predicted h to be proportional to $l_N(N/f)^{-2/3}$ and l to $l_N(N/f)^{1/3}$. Figure 8 shows the observed radius and thickness, normalized by l_N , as a function of N/f for all runs with $N/f > 0.6$. This cutoff value

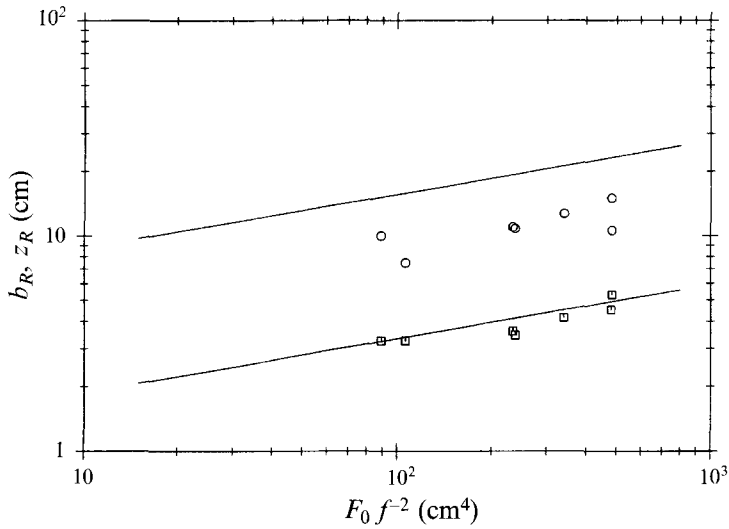


FIGURE 9. The thermal radius b_R (\square) and depth z_R (\circ) at the point of column formation for stratified runs with $N/f < 0.6$. The lines are the results, (25) and (26), from the unstratified runs.

was chosen since for $N/f > 0.6$ there was no evidence of column formation during the sinking phase. Rotation only affected the spreading at the neutral level. Also shown are the best fits of the predicted scalings,

$$l = 0.9l_N(N/f)^{\frac{1}{3}}, \quad (27)$$

$$h = 0.6l_N(N/f)^{-\frac{2}{3}}, \quad (28)$$

giving $k_5 = 0.9$ and $k_6 = 0.6$ in (16) and (17). The agreement, especially for l , is quite good. Fitting without constraining the exponent of N/f gives a coefficient of 0.86 and an exponent of 0.28 for l , and 0.54 and -0.49 , respectively, for h .

All the vortices were axisymmetric and stable. This is consistent with the stability criterion that $l/L_R \lesssim 1$. Using (9), (18), and (27)

$$l/L_R \approx 0.3(N/f)^{-\frac{2}{3}},$$

which for $N/f > 0.6$ is always well below one.

For $N/f < 0.6$, column formation during the falling phase was observed. Figure 9 shows the radius b_R and critical depth z_R of the columns versus $F_0 f^{-2}$. Also shown are the results (25) and (26) from the unstratified runs (cf. figure 4). The radius data agree with the non-stratified results. The trend of the critical depth z_R follows the non-stratified trend, but the depth is about a factor of two smaller with stratification.

The observed thermal vortex radius and thickness after geostrophic adjustment are shown in figure 10. Also shown are the predicted scaling relations derived for $N/f \ll 1$ ((20) and (21)),

$$l = 1.03l_N(N/f)^{\frac{2}{3}}, \quad (29)$$

$$h = 0.52l_N(N/f)^{-\frac{1}{3}}. \quad (30)$$

The agreement is again quite good. Unconstrained fitting gives a coefficient of 0.99 and an exponent of 0.63 for l . For h , the coefficient is 0.48 and exponent is -0.40 . The stability parameter l/L_R is, for l given by (29) and L_R by (18),

$$l/L_R \approx 0.4(N/f)^{-\frac{1}{3}}.$$

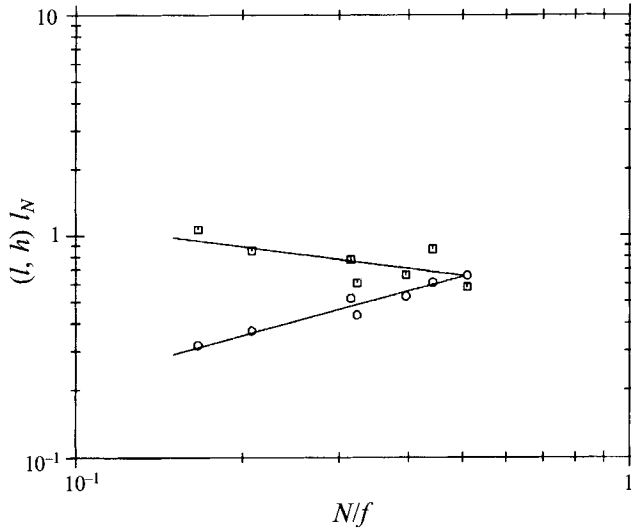


FIGURE 10. Normalized thermal vortex radius l/l_N (\circ) and half-thickness h/l_N (\square) for the runs with $N/f < 0.6$. The lines are the best fits of the proposed scalings, (29) and (30).

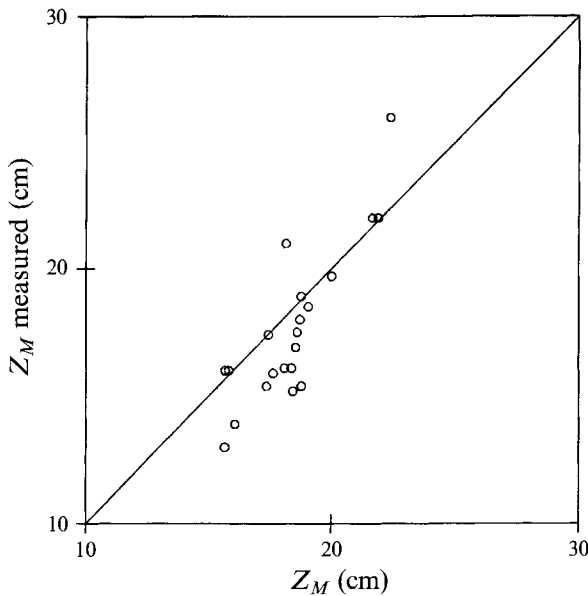


FIGURE 11. The measured neutral buoyancy level versus the non-rotating theory (9).

Instability is expected for $N/f \lesssim 0.06$. The experiments were limited to $N/f \gtrsim 0.16$, and were all stable, consistent with this estimated cut-off.

Finally, figure 11 shows the observed spreading level, defined as the depth of the equator of the thermal vortex, versus the non-rotating prediction (9) for all the stratified experiments. The agreement is satisfactory though there is a tendency to reach a depth slightly less than the predicted level. This is most likely due to the finite initial size of the initial condition. Correction for this effect would work in the direction of improving the agreement. There is no clear dependence on N/f . Thus the assumption that the penetration depth scales with l_N for $N/f \ll 1$ is valid. The total penetration

$Z_M + h$ of the final state will be larger than the non-rotating prediction and will increase as N/f decreases (cf. (28) and (30)).

4. Discussion

Scaling arguments and experiments were used to study the effects of background rotation on the evolution of turbulent thermals. When the background is unstratified thermal evolution is not affected by rotation until the Rossby number $w/fb \approx 0.7$. This occurs at a critical depth $z_R \approx 4.9(F_0 f^{-2})^{1/2}$. The thermal continues to fall without expanding in a Taylor column with radius $b_R \approx 1.1(F_0 f^{-2})^{1/2}$. Rotation prohibits the radial growth and therefore greatly reduces the lateral entrainment. The rate of descent is $w \approx 1.4F_0^{1/2} t^{-1/2}$, independent of f . This independence of f differs from the results of Elrich (1979). However, his experiments were not conclusive and only covered a few values of the relevant parameters. Also, the thermals were initiated by rapid injection with a syringe so that significant initial vertical momentum was introduced.

When the background is stratified, thermal evolution depends on N/f . For $N/f > 0.6$ the thermal reaches the neutral buoyancy level before it is affected by rotation. When $N/f < 0.6$ the thermals fall to form a column before reaching a neutral level. The column radius scaling is the same as for the unstratified case. In either regime, geostrophic adjustment eventually results in a baroclinic vortex pair consisting of an anticyclonic lens of thermal fluid at the neutral level and cyclonic circulation above. The adjusted thermal lens has a Burger number $Nh/fl \sim 1$. However, the scalings for the lens thickness $2h$, radius l , and vortex stability criterion are different in the two regimes.

The transition between regimes at $N/f \approx 0.6$ can be understood by examining the ratio of the critical column depth z_R (12) to the depth of the neutral buoyancy level Z_M (9),

$$z_R/Z_M = 1.86(N/f)^{1/2}.$$

This suggests that for $N/f < 0.29$ a column will form before the thermal reaches the neutral level. This value is close to the observed value of 0.6. It is also interesting to note that the transition is independent of F_0 . For a thermal in an unstratified fluid the total depth H replaces Z_M and the analogous ratio z_R/H is not independent of F_0 .

These experiments emphasize the isolated nature of the columns. Once radial spreading has stopped, the lateral entrainment is significantly reduced. This implies that a field of convective columns, as found in the deep convection studies, will interact very weakly. Fluid that eventually reaches the bottom will originate from above the critical depth for column formation. Fluid between columns will rise vertically to replace fluid entrained into the columns near the surface. If the ambient fluid is stratified the mixed-layer depth $z \sim (B_0 t)^{1/2}/N$. At $t \sim f^{-1}$, $z = z_0 \sim (B_0/fN^2)^{1/2}$. Further deepening of the mixed layer should be inhibited by stratification and geostrophic adjustment and instability of the whole convecting region. Whether convective columns form should depend on the ratio of the unstratified critical depth $z_c \sim (B_0 f^{-3})^{1/2}$ to z_0 : $z_c/z_0 \sim N/f$. For $N/f \ll 1$ convective columns are likely to form and when $N/f \gg 1$ they are unlikely. Again the transition is independent of the buoyancy flux.

The experiments show that vortices with features similar to megaplume observations are generated by a thermal release. Megaplume 1 observed by Baker *et al.* (1989) over the Juan de Fuca Ridge was centred about 700 m above the bottom. The lens had a thickness $2h \approx 700$ m and a radius of 7000 m. The ambient buoyancy frequency $N \approx 10^{-3} \text{ s}^{-1}$ and $f = 10^{-4} \text{ s}^{-1}$. These give $N/f \approx 10$ and $Nh/fl \approx 0.5$. Using the relation for the lens radius in the strong stratification regime (27) an estimate for F_0 is

$1.7 \times 10^8 \text{ m}^4 \text{ s}^{-2}$. A release of this magnitude is expected to rise to a neutral level of about 10^5 m above the source. This is much too large. The failure of the scaling is most likely due to the assumption of an instantaneous release from a source with a lengthscale much less than l_N . The hydrothermal release that generated the megaplume is probably not instantaneous and occurs over a finite area (Baker *et al.* 1989). An investigation into the roles of the source timescale and lengthscale on vortex generation is underway.

This work was supported by an NSF Ridge Program grant (OCE 92-16628). W. Williams, B. Racine and R. Frazel helped with the experiments. The author thanks John Marshall for several helpful discussions. Woods Hole Oceanographic Institution Contribution No. 8252.

REFERENCES

- BAKER, E. T., LAVELLE, J. W., FEELY, R. A., MASSOTH, G. J. & WALKER, S. L. 1989 Episodic venting of hydrothermal fluids from the Juan de Fuca Ridge. *J. Geophys. Res.* **94**, 9237–9250.
- CHADWICK, W. R., EMBLEY, R. W. & FOX, C. G. 1991 Evidence for volcanic eruption on the southern Juan de Fuca Ridge between 1981 and 1987. *Nature* **350**, 416–418.
- ELRICK, J. R. 1979 Interaction between a discrete downdraft and a rotating environment. *J. Atmos. Sci.* **36**, 306–312.
- FERNANDO, H. J. S., CHEN, R.-R. & BOYER, D. L. 1991 Effects of rotation on convective turbulence. *J. Fluid Mech.* **228**, 513–547.
- GASCARD, J.-C. 1978 Mediterranean deep water formation – baroclinic instability and oceanic eddies. *Oceanol. Acta* **1**, 315–330.
- GILL, A. E. 1981 Homogeneous intrusions in a rotating stratified fluid. *J. Fluid Mech.* **103**, 275–296.
- GRIFFITHS, R. W. & LINDEN, P. F. 1981 The stability of vortices in a rotating, stratified fluid. *J. Fluid Mech.* **105**, 283–316.
- HELFRICH, K. R. & BATTISTI, T. M. 1991 Experiments on baroclinic vortex shedding from hydrothermal plumes. *J. Geophys. Res.* **96**, 12511–12518.
- HELFRICH, K. R. & SEND, U. 1988 Finite-amplitude evolution of two-layer geostrophic vortices. *J. Fluid Mech.* **197**, 331–348.
- JONES, H. & MARSHALL, J. 1993 Convection with rotation in a neutral ocean; a study of open-ocean deep convection. *J. Phys. Oceanogr.* **23**, 1009–1039.
- MAXWORTHY, T. & NARIMOUSA, S. 1993 Unsteady deep convection in a homogeneous rotating fluid. *J. Phys. Oceanogr.* in press.
- MORTON, B. R., TAYLOR, G. J. & TURNER, J. S. 1956 Turbulent gravitational convection from maintained and instantaneous sources. *Proc. R. Soc. Lond. A* **234**, 1–23.
- SANCHEZ, O., RAYMOND, D. J., LIBERSKY, L. & PETSCHKE, A. G. 1989 The development of thermals from rest. *J. Atmos. Sci.* **46**, 2280–2292.
- SCHOTT, F. & LEAMAN, K. D. 1991 Observations with moored acoustic doppler current profilers in the convection regime in the Gulf du Lion. *J. Phys. Oceanogr.* **21**, 558–574.
- SCORER, R. S. 1957 Experiments on convection of isolated masses of buoyant fluid. *J. Fluid Mech.* **2**, 583–594.
- SPEER, K. G. 1989 A forced baroclinic vortex around a hydrothermal plume. *Geophys. Res. Lett.* **16**, 461–464.
- STOMMEL, H., VOORHIS, A. & WEBB, D. 1971 Submarine clouds in the deep ocean. *Am. Scientist* **59**, 717–723.
- TURNER, J. S. 1973 *Buoyancy Effects in Fluids*. Cambridge University Press.
- TURNER, J. S. 1986 Turbulent entrainment: the development of the entrainment assumption, and its application to geophysical flows. *J. Fluid Mech.* **173**, 431–472.
- WILKINS, E. M., SASAKI, Y. K., FRIDAY, E. W., MCCARTHY, J. & MCINTYRE, J. R. 1969 Properties of simulated thermals in a rotating fluid. *J. Geophys. Res.* **74**, 4472–4486.